

UNSTEADY CONVECTIVE HEAT TRANSFER MODELING AND APPLICATION TO ENGINE INTAKE MANIFOLDS

Pin Zeng, Dennis N. Assanis

Automotive Research Center, University of Michigan, Ann Arbor, MI 48109, USA

ABSTRACT

Unsteadiness is an important feature of heat transfer in engine manifolds. In order to understand how unsteadiness affects heat transfer, the authors developed two-stage unsteady models based on dimensional analysis of the boundary layer momentum equation and a turbulent decay relation. In Stage I, the heat transfer rate exhibits a phase delay from the velocity variation. Hence, the heat transfer coefficient is not only a function of Reynolds and Prandtl numbers, but also a function of the velocity changing rate. In Stage II, the heat transfer rate experiences a decay process related to a turbulence decay process. A fundamental pipe flow device was established to identify the criterion of dividing the two-stage heat transfer process and validate the unsteady heat transfer models. The validated unsteady heat transfer models were applied to the heat transfer analysis of an engine intake manifold. Unsteady model predictions agree well with measured heat transfer data.

1. INTRODUCTION

Heat transfer is an important process in the intake manifold of engines. It increases the intake air temperature which reduces the volumetric efficiency and the tolerance to engine knock, and causes higher chemical reaction rates leading to increased NOx emissions. It also affects engine performance and emissions through enhancing fuel evaporation and charge mixing in the engine intake ports and cylinders.

Because a correlation type, easy-to-use unsteady heat transfer model is not available, classical, steady correlations in the form of $Nu = a Re^b$ or $Nu = a Re^b Pr^n$ are widely used for estimating convective heat transfer coefficient in the intake manifolds of engines [1 to 4]. The constants a and b are adjusted to match the experimental data to account for unsteady heat transfer enhancements, surface deposits, and surface roughness. Examples of those correlations are listed below:

Ditus and Boelter [1]

$$Nu = 0.023 Re^{0.8} Pr^n \quad (1)$$

Bauer et al. [2]

$$Nu = 0.062 \overline{Re}^{0.73} \quad \text{for straight manifold} \quad (2)$$

$$Nu = 0.140 \overline{Re}^{0.66} \quad \text{for curved manifold} \quad (3)$$

Depcik and Assanis [3]

$$Nu = 0.070 \overline{Re}^{3/4} \quad (4)$$

Shayler et al. [4]

$$Nu = 0.135 \overline{Re}^{0.713} \quad (5)$$

These correlations provide reasonable agreement with experimental data in fully-developed steady pipe flows and acceptable agreement with time-resolved experimental data in unsteady flows with slow velocity variation under the quasi-steady assumption. However, for highly unsteady flows with rapid velocity variation, such as engine flows, these correlations can produce large errors in both phase and magnitude. Experimental results published by different researchers show that the unsteady flow effect in the engine intake manifold enhances heat transfer by 50% to 100 % over the prediction of the steady pipe flow correlation of Eq. (1). At different engine speed and load conditions, the unsteadiness of the flow condition is different. Therefore, the constants a and b are usually optimized only for one operating condition of a given engine, and hence compromised for other conditions. If an unsteady heat transfer correlation could be

developed accounting for the unsteady flow effect, the accuracy of the heat transfer prediction in the engine intake manifold could be improved. This provides the impetus for the authors to develop such an unsteady heat transfer correlation.

Because of the difficulties in measuring instantaneous heat transfer in unsteady flows with rapid velocity variation, only a few experimental results have been published [2 and 5]. The mechanism of how unsteadiness affects heat transfer is still under development. A recent study published by the authors of this paper [6] developed an unsteady heat transfer correlation through dimensional analysis of the boundary layer momentum equation. In that paper, the unsteady heat transfer process in the engine manifold was divided into two stages, Stage I where heat transfer is delayed from velocity variation and Stage II where heat transfer experiences a gradual decay process. Predictions of unsteady heat transfer during Stage I agreed well with the experimental results published by Bauer et al. [2]. However, the study did not address how to identify the onset of Stage II and how to calculate the turbulence intensity in Stage II.

In this paper, the authors present three sets of unsteady heat transfer measurements acquired in a fundamental pipe flow device. From the experimental data, a criterion to identify the onset of the heat transfer decay process (Stage II) is developed. Using the CFD results of Malan and Johnston [7] which demonstrated that the length scale of the large eddies is constant during the turbulence decay process, a simple equation that calculates the turbulence intensity in the decay process was derived. Finally, the heat transfer correlation developed by Malan and Johnston [7] was adopted to calculate the unsteady heat transfer rate during the turbulence decay process.

This paper is organized into 5 sections. Followed by this introductory section, Section 2 presents the derivation of the unsteady heat transfer models. Section 3 demonstrates the validation of the unsteady heat transfer models. Section 4 applies the unsteady heat transfer models to an engine intake manifold. Finally, section 5 concludes the study.

NOMENCLATURE

- D : hydraulic diameter of the pipe
 C_f : skin friction coefficient
 k : thermal conductivity of the gas
 L : length scales
 $Nu \equiv hL/k$: Nusselt number
 $Pr \equiv \nu/\alpha$: Prandtl number
 $Re \equiv UL/\nu$: Reynolds number
 T_g, T_w : gas (air) and wall temperatures
 U : characteristic velocity (root mean square value of the instantaneous velocity)
 u' : turbulence intensity (root mean square value of the fluctuating velocity component)

Greek symbols

- α : thermal diffusivity of the gas
 ρ : density of the gas
 ν : kinetic viscosity of the gas
 $\Pi \equiv (L/U^2)(dU/dt)$: dimensionless variable to characterize the unsteady behavior of the momentum boundary layer

Subscript

- ∞ : far field, outside boundary layer
 dcy : variables during turbulence decay process
 dyn : dynamic variables
 sty : steady variables
 t : turbulent variables

2. DERIVATION OF UNSTEADY HEAT TRANSFER MODELS

The experimental results presented later in the section 3 of this paper indicate the existence of the two stages of the unsteady heat transfer process. These results are also consistent with the heat transfer experimental results of Bauer et al. [2] for the engine intake manifold shown in the section 4 of this paper. According to these experimental results, the two-stage unsteady heat transfer models are developed below.

Stage I: Dimensional analysis of boundary layer momentum equation

Under the assumption of incompressible and uniform pressure field, the time-averaged momentum equation for the unsteady boundary layer shown in Fig. 1 can be written as

$$\frac{\partial \bar{u}}{\partial t} + \bar{u} \frac{\partial \bar{u}}{\partial x} + \bar{v} \frac{\partial \bar{u}}{\partial y} = \nu \frac{\partial^2 \bar{u}}{\partial y^2} \quad (6)$$

Equation (6) can be normalized using the dimensionless variables defined in Eq. (7).

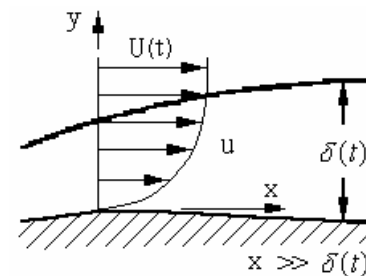


Fig. 1 Unsteady momentum boundary layer

$$\left. \begin{aligned} u^* &= \bar{u}/U, \quad v^* = \bar{v}/U \quad \text{where } U = U(t) \\ u^* &= x/L, \quad v^* = y/L \\ t^* &= t/(L^2/\alpha) = \text{Fourier number} \end{aligned} \right\} \quad (7)$$

The normalized momentum equation can be expressed as

$$\left\langle \frac{L}{U^2} \frac{dU}{dt} \right\rangle u^* + \frac{1}{Re Pr} \frac{\partial u^*}{\partial t^*} + u^* \frac{\partial u^*}{\partial x^*} + v^* \frac{\partial u^*}{\partial y^*} = \frac{1}{Re} \frac{\partial^2 u^*}{\partial y^{*2}} \quad (8)$$

Three dimensionless variables can be found from Eq. (8) to be

$$Re \equiv \frac{UL}{\nu}, \quad Pr \equiv \frac{\nu}{\alpha} \quad \text{and} \quad \boxed{\Pi \equiv \frac{L}{U^2} \frac{dU}{dt}}, \quad (9)$$

where Reynolds and Prandtl numbers Re and Pr are commonly used in steady heat transfer correlations, and Π is a new dimensionless variable that relates to the unsteady boundary layer. Its physical meaning may be expressed as

$$\begin{aligned} \Pi &\equiv \frac{L}{U^2} \frac{dU}{dt} = \frac{\rho \frac{dU}{dt}}{\rho U \frac{U}{L}} \\ &= \frac{\text{temporal gradient of inertial force}}{\text{spatial gradient of inertial force}} \end{aligned} \quad (10)$$

The authors introduced the dynamic variable concept to extend any steady correlation to unsteady form. The dynamic velocity U_{dyn} for convective heat transfer can be constructed using the dimensionless variable defined in Eq. (11) as

$$U_{dyn} = U(1 + C_2 \Pi) = U \left(1 + C_2 \frac{L}{U^2} \frac{dU}{dt} \right), \quad (11)$$

where C_2 is a calibration constant that needs to be determined experimentally. Then, the dynamic Reynolds number Re_{dyn} can be constructed using the dynamic velocity U_{dyn} .

$$\begin{aligned} Re_{dyn} &= \frac{U_{dyn} L}{\nu} = \frac{UL}{\nu} (1 + C_2 \Pi) \\ &= Re \left(1 + C_2 \frac{L}{U^2} \frac{dU}{dt} \right) \end{aligned} \quad (12)$$

In steady flows, the skin friction coefficient can be calculated using

$$\left(\frac{1}{2} C_f \right) = C_1 Re^{-\beta}, \quad (13)$$

where C_1 is a calibration constant. According to Moody's chart, in smooth pipes, $\beta = 1$ for laminar flow, $\beta = 1/4$ for $Re \leq 2 \times 10^4$ and $1/5$ for $Re \geq 2 \times 10^4$ turbulent flows. For flows over a flat wall, $\beta = 0.5$ for both laminar and turbulent flows. Similarly, the dynamic skin friction coefficient can be constructed using the dynamic Reynolds number Re_{dyn} .

$$\begin{aligned} \left(\frac{1}{2} C_f \right)_{dyn} &= C_1 Re_{dyn}^{-\beta} \\ &= C_1 Re^{-\beta} \left(1 + C_2 \frac{L}{U^2} \frac{dU}{dt} \right)^{-\beta} \end{aligned} \quad (14)$$

The Colburn analogy for unsteady heat transfer can be constructed using dynamic variables as

$$St_{dyn} Pr^{2/3} = \frac{Nu_{dyn}}{Re_{dyn} Pr^{1/3}} = \left(\frac{1}{2} C_f \right)_{dyn}. \quad (15)$$

Finally, the unsteady heat transfer correlation is derived by substituting Eq. (14) into Eq. (15), i.e.

$$\begin{aligned} Nu_{dyn} &= C_1 Re_{dyn}^{1-\beta} Pr^{1/3} \\ &= C_1 Re^{1-\beta} Pr^{1/3} \left(1 + C_2 \frac{L}{U^2} \frac{dU}{dt} \right)^{1-\beta} \end{aligned} \quad (16)$$

Equation (16) shows that the unsteady heat transfer coefficient is not only a function of Reynolds and Prandtl numbers, but also a function of velocity changing rate. It is made up by a steady solution and an unsteady velocity correction term, as shown in Eq. (17).

$$\begin{aligned} Nu_{dyn} &= \underbrace{C_1 Re^{1-\beta} Pr^{1/3}}_{\text{steady solution}} \underbrace{\left(1 + C_2 \frac{L}{U^2} \frac{dU}{dt} \right)^{1-\beta}}_{\text{unsteady correction}} \\ &= Nu_{sty} \underbrace{\left(1 + C_2 \frac{L}{U^2} \frac{dU}{dt} \right)^{1-\beta}}_{\text{unsteady correction}} \end{aligned} \quad (17)$$

The steady solution Nu_{sty} can be obtained from the Colburn correlation, or any other existing steady-state heat transfer correlations. The constant C_1 comes from the steady heat transfer correlations used. The constant C_2 should be negative. When velocity increases, the value of the correction term becomes less than one; hence, it reduces the prediction of heat transfer from the steady solution. When velocity decreases, the value of the correction term becomes larger than one, thus increasing the prediction of heat transfer from the steady solution. In this way, the unsteady velocity correction term simulates the phase delay for the turbulence intensity and heat transfer from the velocity variation. At the limit of steady flow condition, $dU/dt \rightarrow 0$, all dynamic variables collapse to their steady values; and the unsteady heat transfer correlation, Eqs. (16) and (12) collapses to the steady solution. The derivation of Eq. (17) is similar to the one presented in [6].

Stage II: Modeling of turbulence decay process

Under the assumption of homogenous and isotropic turbulence, the turbulence decay can be evaluated using the turbulence decay relation:

$$\frac{d u_{\infty}'^2}{dt} = -\frac{A u_{\infty}'^3}{L_{\infty}} \quad (18)$$

where A is a constant of order one (Batchelor [8], page 106 and Heywood [9], page 336) and L_{∞} is the large eddy length scale. The CFD results of Malan and Johnston [7] show that L_{∞} is almost constant during the turbulence decay process.

Then, Eq. (18) can be integrated to get

$$u_{\infty}' = \frac{1}{(A/2L_{\infty})t + 1/u_{\infty}'(0)}. \quad (19)$$

Equation (19) implies that the turbulence decay process outside the boundary layer is independent of the fluid properties and only depends on the initial turbulence intensity $u_{\infty}'(0)$ when the decay process starts. This is because the viscous effects can be neglected outside the boundary layer. The large eddy length scale L_{∞} is assumed to be proportional to the integral length scale, which is the diameter D for the pipe flows. $L_{\infty} = C_l \times D$. The constant $C_l = 0.03$ is found to best fit the experimental results.

The heat transfer correlation developed by Malan and Johnston [7] for the shear-free boundary layer heat transfer is adopted to predict the heat transfer coefficient in the heat transfer decay process, i.e.

$$Nu_{dcy} = 0.333 Re_{t,\infty}^{3/4} \quad (20)$$

where $Re_{t,\infty} = u' L_{\infty} / \nu$ is the turbulent Reynolds number outside of the shear-free boundary layer.

3. VALIDATION OF UNSTEADY HEAT TRANSFER MODELS

In this section, a turbulent pipe device shown in Fig. 2 is established to carry out unsteady heat transfer experiments. An air tank, a ball valve, a long stainless steel pipe and sensors are used to build the device. A TSI 1210 hotwire probe, a MEDTHERM air temperature thermocouple and a MEDTHERM heat flux sensor are installed at the same cross section, 2 ft from the exit of the pipe. The hotwire probe and air temperature sensor are used to measure the air velocity and air temperature in the pipe center line. The heat flux sensor is used to measure the instantaneous surface heat flux from two thermocouples; one installed on the front surface and one on the backside, 3 mm from the front surface. Three surface thermocouples are installed on the outer surface of the pipe to monitor the temperature difference along the pipe. Compressed air at room temperature comes into the air tank from a hand-controlled valve monitored and controlled by a pressure gauge.

Before each test, the ball valve is opened and the air in the tank flows into the pipe. The pipe surface temperature is heated to over 90 °C using two fire torches through pipe heating holes on both sides of the pipe. The hotwire and gas temperature sensors are removed from the pipe to prevent them being damaged from the pipe heating process. After installing the hotwire and gas temperature sensors, the test can be started. By hitting the handle of the ball valve using a hammer, the ball valve is suddenly opened and then immediately closed by the pull back force of the rubber band. It creates a pulsation type, unsteady air flow that is similar to the air flow in the engine manifolds. The time constants for the hotwire, gas temperature thermocouple and the surface heat flux sensors are 0.5 ms, 1~2 ms and $\sim 1 \mu s$ respectively. The errors for these sensors are 5%, ± 1 °C and 5% under steady measurement conditions. Under unsteady measurement conditions, the error of the hotwire sensor can be as high as 15%. A data acquisition system with 14-bit vertical resolution is used for this project. The 10 kHz wide band, 5B series signal conditioning modules are used to amplify and filter the signals to increase the signal-to-noise ratio for the air temperature and heat flux measurements. A more detailed description of the experimental set is presented in Zeng [10].

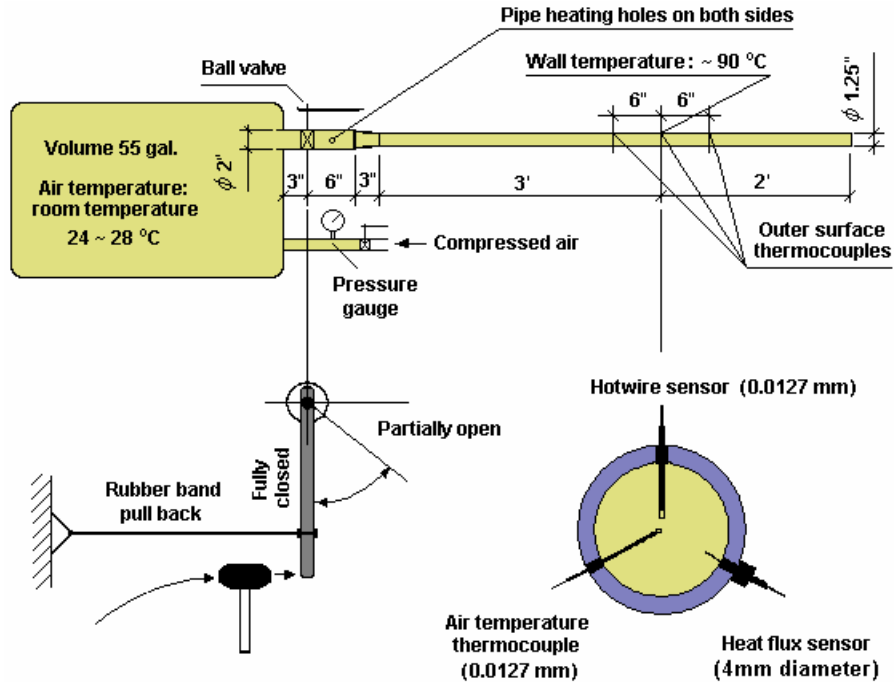


Fig. 2 Fundamental pipe flow device for unsteady heat transfer experiments

Predictions based on steady heat transfer correlation

Comparisons of measured heat flux with predictions based on the steady, Ditus-Boelter heat transfer correlation (Eq. 1), are shown in Figs. 3 to 5.

Note that as the main flow duration increases from ~24 ms to ~90 ms, the changing rate of the velocity increases, i.e. the unsteadiness of the flow increases. When the ball valve on the pipe flow device suddenly opens and closes, the air velocity measured using the hotwire probe in the pipe rapidly increases and decreases during main flow duration. After the air velocity drops to ~ zero, the flow starts to oscillate in the pipe. The unsteady flow in the pipe creates unsteady convective heat transfer between the air and the inner surface of the pipe. It can be seen that the measured results exhibit a phase delay relative to the predictions by the steady heat transfer correlation during air velocity increase and the early part of velocity decrease. In the later part of the air velocity decrease, the heat flux does not follow the decrease of the air velocity; instead, it starts a gradually decaying process. This indicates that prediction of unsteady heat flux using steady heat transfer correlations can produce large errors in both the phase and the magnitude. Thus, unsteady heat transfer models need to be developed to simulate the unsteady heat transfer process.

Predictions based on unsteady heat transfer models

Using the Ditus-Boelter correlation as the steady solution for the case of $T_w > T_g$ and the length scale to be the pipe diameter D , then, Eq. (17) becomes

$$Nu_{dyn} = \underbrace{0.023 Re^{0.8} Pr^{0.4}}_{\text{steady solution}} \underbrace{\left(1 - 0.75 \frac{D}{U^2} \frac{dU}{dt}\right)^{0.8}}_{\text{unsteady correction}} \quad (21)$$

The constant $C_2 = -0.75$ has been selected to give the best agreement between the predicted unsteady heat flux and the experimental data. The negative value of C_2 makes a negative correction on the prediction of the steady solution during velocity increases and a positive correction during velocity decreases. Therefore, the unsteady correction term creates a phase lag compared to the prediction of the steady solution. The comparison between the measured and the predicted results by Eq. (21) are shown in Figs. 6 to 8. In order to make the figures less crowded, the predictions of the steady correlation are turned off after the flows start to oscillate.

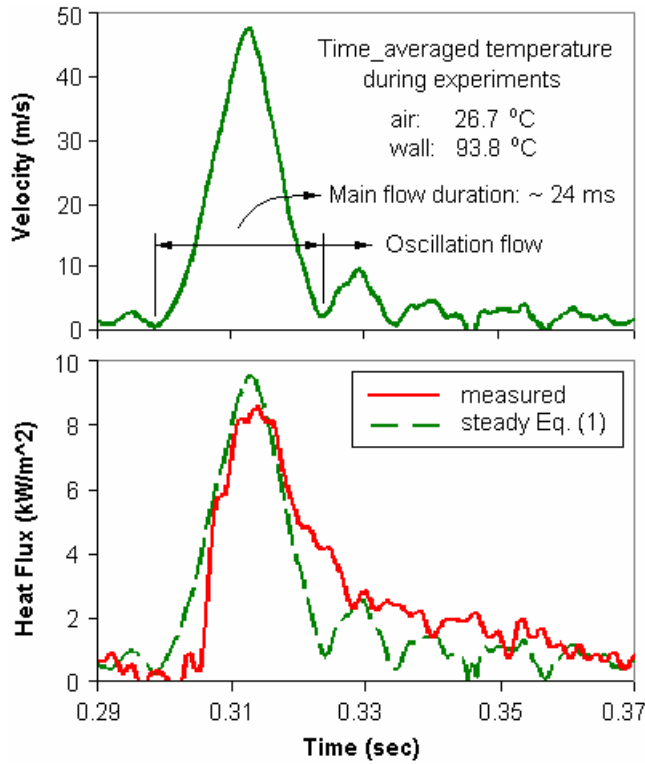


Fig. 3 Air velocity and surface heat flux in case 1

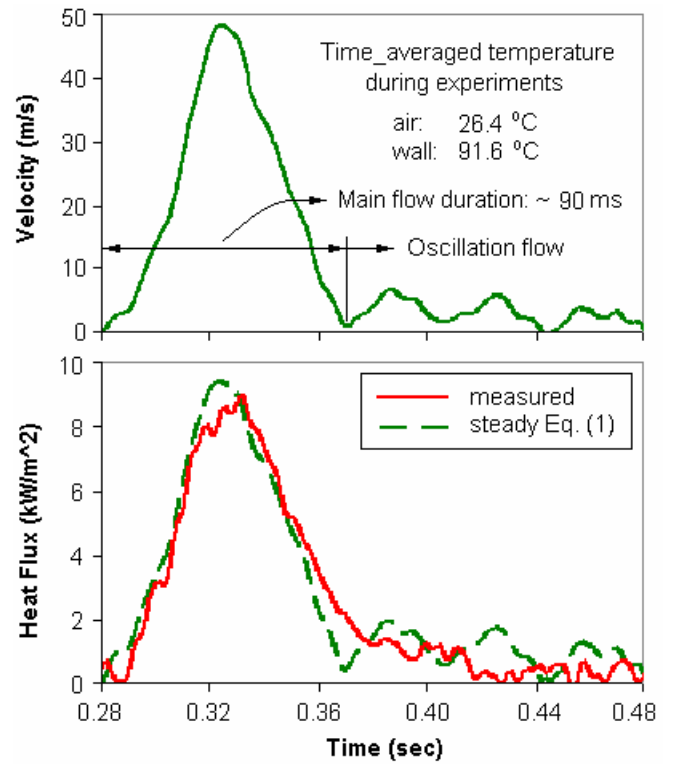


Fig. 5 Air velocity and surface heat flux in case 3

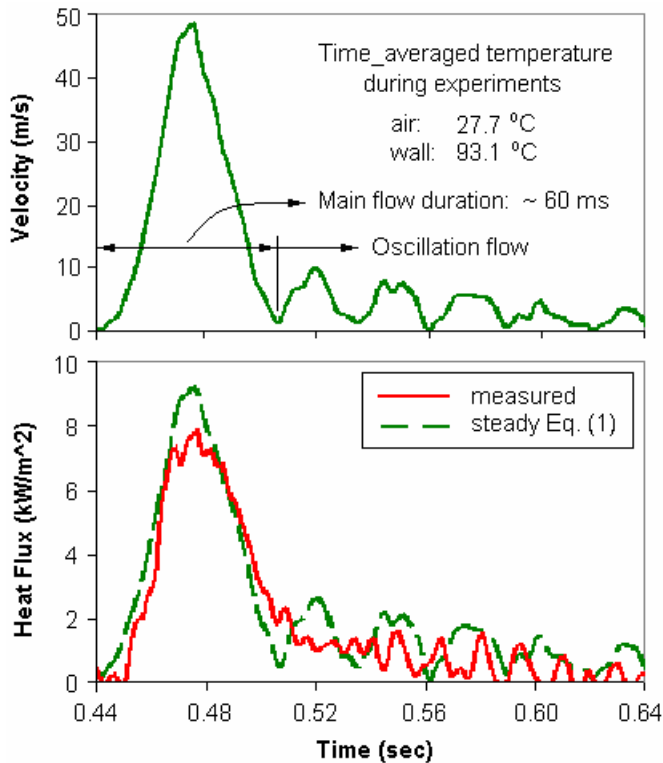


Fig. 4 Air velocity and surface heat flux in case 2

Equation (21) can correct the phase delay of the heat flux relative to the main flow velocity variation during the air velocity increase and the early part of the velocity decrease. However, as the air velocity continues to decrease beyond a critical value, the prediction of the unsteady heat transfer correlation starts to deviate from the measured heat flux. Our experimental results suggest that this occurs when

$$\Pi|_{critical} = \left(\frac{D}{U^2} \frac{dU}{dt} \right)_{critical} = -0.7 \sim -0.8. \quad (22)$$

Equation (22) defines a criterion for the onset of the turbulence decay-driven heat transfer process. During the period when the velocity of the main flow decreases, the value of Π changes from higher to lower than the critical value. This transition demarks the shift of the heat transfer process from Stage I into Stage II. In Stage I of the unsteady heat transfer process, the measured heat flux has a phase delay from the velocity variation. In Stage II of the unsteady heat transfer process, the measured heat flux does not follow the decreasing process of the velocity and experiences a decay process. During the latter, heat transfer cannot be correlated to mean flow velocity. Instead, the authors postulate that the turbulence decay is the dominant factor in the Stage II heat transfer and correlate the heat transfer directly to turbulent intensity.

Simulation of the heat transfer decay process

The turbulent decay model described by Eqs. (19) and (20) can be used to predict the unsteady heat transfer coefficient in Stage II. When $\Pi = \Pi|_{critical}$, the heat transfer is continuous. The heat transfer coefficient can be calculated using either Eq. (21) or Eq. (20). Then, the continuity condition can be used to calculate the initial turbulence intensity $u'_{\infty}(0)$ at the beginning of the turbulent decay process. From $u'_{\infty}(0)$ the turbulence intensity u'_{∞} during the turbulence decay process can be calculated using Eq. (19). Finally, from u'_{∞} and Eq. (20), the heat transfer coefficient and the heat flux during turbulence decay process can be predicted.

Figures 6 to 8 show that predictions based on the proposed unsteady heat transfer models agree well with the experimental data for the entire unsteady heat transfer process. This validates that the unsteady heat transfer models developed in this paper are capable of capturing the characteristics of the unsteady heat transfer process. The results also indicate that as the main flow duration increases, the flow unsteadiness decreases and the percentage of heat transfer in the heat transfer decay process decreases. Under those conditions, the unsteady heat transfer enhancement decreases, and discrepancies between experimental data and the prediction based on steady correlations decrease.

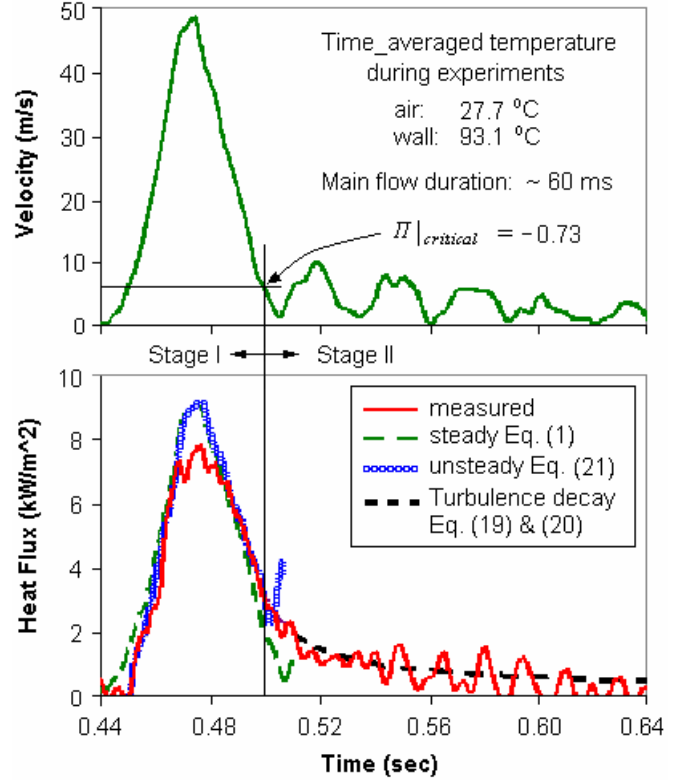


Fig. 7 Air velocity and surface heat flux in case 2

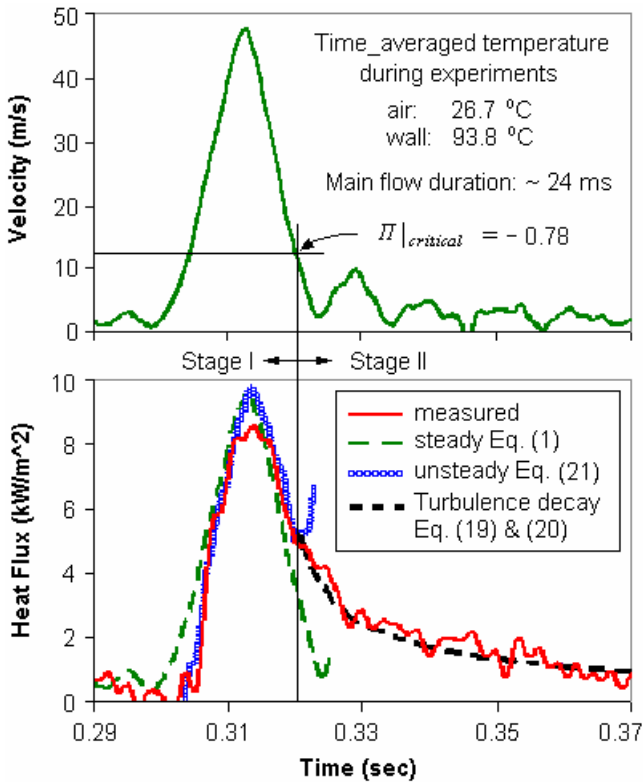


Fig. 6 Air velocity and surface heat flux in case 1

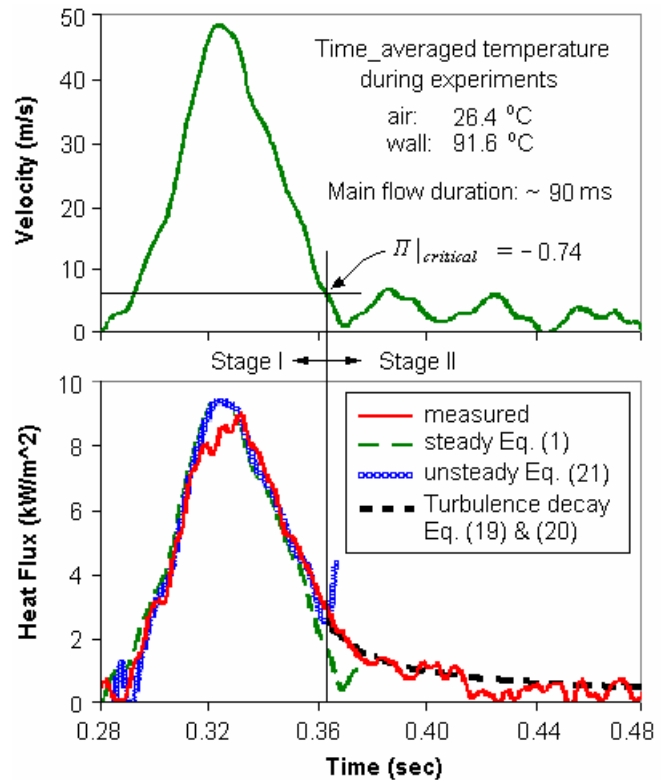


Fig. 8 Air velocity and surface heat flux in case 3

In this way, the unsteady heat transfer models, including Eqs. (17) to (20) are validated in a fundamental pipe flow heat transfer device.

4. APPLICATION OF UNSTEADY HEAT TRANSFER MODELS TO THE ENGINE INTAKE MANIFOLD

The unsteady heat transfer models developed and validated in the above sections are applied to the experimental data taken by Bauer et al. in the intake manifold of a spark-ignition engine [2]. Figure 9 compares the experimental data with predictions based on steady and unsteady heat transfer models. Fig. 9 (a) focus on the intake process during the intake valves open and close. Fig. 9 (b) covers the heat transfer for the entire engine working cycle (720 degree) to show the heat transfer decay process.

It can be seen that the steady model Eq. (1), the Ditus and Boelter correlation, overestimated the peak heat flux comparing to the experimental result. To match the peak heat flux value

for the steady correlation, the constant C_1 is adjusted from 0.023 to 0.018. Then the heat transfer in the Stage I can be calculated using

$$Nu = 0.018 Re^{0.8} Pr^{0.4} \left(1 - 0.75 \frac{D}{U^2} \frac{dU}{dt} \right)^{0.8} \quad (23)$$

Similar to the calculation process presented in Section 3, Eq. (22) is used to identify the onset of the heat transfer decay process, and Eqs. (19) and (20) are used to calculate the heat flux during the turbulent and heat transfer decay process. Once again, the unsteady heat transfer model predictions agree well with the experimental data.

The unsteady heat transfer models predicted the phase delay of heat transfer from the velocity variation in the Stage I and captured the main characteristics of the heat transfer decay process in the Stage II.

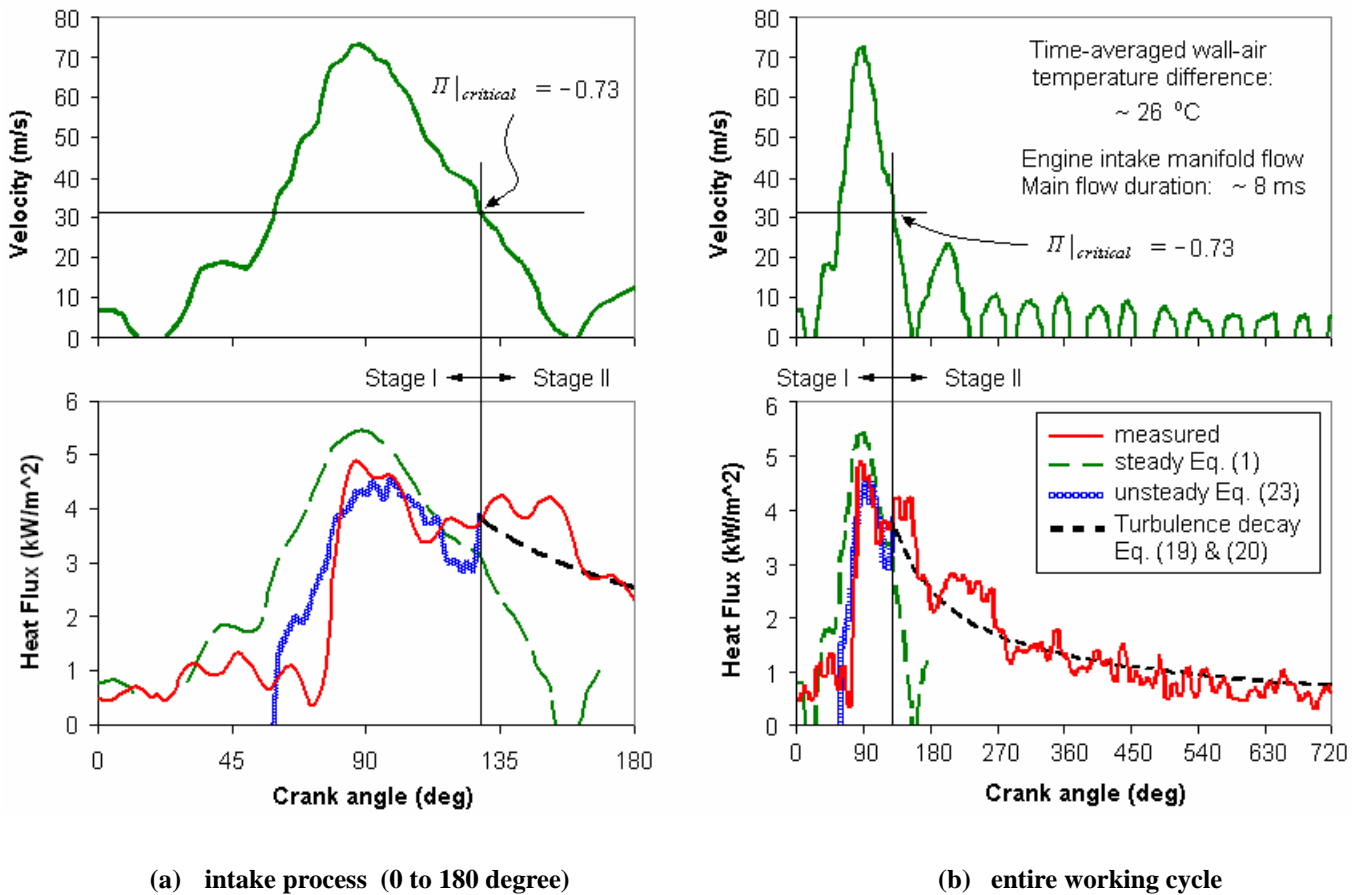


Fig. 9 Air velocity and surface heat flux measurements by Bauer et al. [2] compared against model predictions

5. CONCLUSIONS

Unsteady flow effect creates both phase and magnitude errors in heat flux predictions based on steady-flow correlations. When the velocity rapidly increases or decreases, heat transfer has a phase delay from the velocity variation. The classical, steady pipe flow heat transfer correlations do not capture the observed phase delay. The unsteady heat transfer correlation, Eq. (17), presented in this paper can be used to shift the heat transfer coefficient predicted by the steady heat transfer correlations to correct for the phase error.

The unsteady heat transfer correlation indicates that the heat transfer coefficient is not only a function of Reynolds and Prandtl numbers, but also a function of the changing rate of velocity. At the limit of steady condition, the unsteady heat transfer correlation collapses to the steady correlation.

When the velocity decreases too fast, so that a criterion (critical value) expressed by Eq. (22) is reached, the heat transfer starts a gradual decay process. Therefore, Eq. (22) divides the unsteady heat transfer process into two stages. During the turbulence decay process (Stage II), heat transfer is independent of the velocity variation, and thus cannot be accounted by steady heat transfer correlations. Instead, it can be correlated to the decaying turbulence intensity expressed by Eq. (19). Finally, Eq. (20) adopted from Malan and Johnston [6] can be used to evaluate the heat transfer in Stage II of the unsteady heat transfer process.

The comparisons between the experimental data and the predictions based on the unsteady heat transfer models agree well for both the pipe flow device and the engine intake manifold. It can be concluded that the study presented in this paper draws a clearer picture for the unsteady heat transfer process and provides solutions to describe and simulate the unsteady heat transfer process.

ACKNOWLEDGMENTS

This study has been sponsored by the Automotive Research Center at the University of Michigan. We are grateful to Dr. Alex Alkidas of General Motors R&D Center for providing hotwire devices and valuable input for this study. We would also like to help Dr. Zoran Filipi of the University of Michigan for his suggestions and help.

REFERENCES

1. Dittus P. W. and L. M. K. Boelter, "Heat Transfer in Automobile Radiators of the Tubular Type," Univ. of California Pub. Eng., Vol. 2, No. 13, p.443-461, 1930
2. Bauer W. D., Wenisch J. and J. B. Heywood, "Averaged and Time-Resolved Heat Transfer of Steady and Pulsating Entry Flow in Intake Manifold of a Spark-Ignition Engine," *Int. J. Heat and Fluid Flow*, 19, pp.1-9, 1998
3. Depcik C. and D. N. Assanis, "A Universal Heat Transfer Correlation for Intake and Exhaust Flows in an Spark Ignition Internal Combustion Engine," SAE 2002-01-0372, 2002
4. Shayler P. J., Colechin M. J. F. and A. Scarisbrick, "Heat Transfer Measurements in the Intake Port of a Spark Ignition Engine," SAE 960273, 1996
5. Barker, A. R. and J. E. F. Williams, "Transient Measurements of the Heat Transfer Coefficient in Unsteady, Turbulent Pipe Flow," *Int. J. Heat and Mass Transfer*, 43, p.3197-3207, 2000
6. Zeng, P. and D. N. Assanis, "Time-Resolved Heat Transfer in Engine Intake Manifold," *Proceedings of the International Symposium on Transient Convective Heat and Mass Transfer in Single and Two-Phase Flows*, Cesme, Turkey, pp.167-176, 2003
7. Malan P. and J. P. Johnston, "Heat Transfer in Shear Free Turbulent Boundary Layers," Stanford University, Stanford, CA, Report MD-64. 1993
8. Batchelor G. K., *The Theory of Homogeneous Turbulence*, Cambridge University Press, Cambridge, 1953
9. Heywood J. B., *Internal Combustion Engine Fundamentals*, Mc-Graw Hill Book Co., New York, 1988
10. Zeng, P., "Unsteady Convective Heat Transfer Modeling and Application to Internal Combustion Engines," PhD thesis, University of Michigan at Ann Arbor, 2004